This article has been accepted for publication in IEEE/OSA Journal of Lightwave Technology. This is the author's version which has not been fully edited and content may change prior to final publication. Citation information: DOI 10.1109/JLT.2022.3197366

High-Cardinality Geometrical Constellation Shaping for the Nonlinear Fibre Channel

Eric Sillekens, *Member, IEEE,* Gabriele Liga, *Member, IEEE,* Domaniç Lavery, *Member, IEEE,* Polina Bayvel, *Fellow, IEEE,* and Robert. I. Killey, *Fellow, IEEE*

***Abstract*—This paper presents design methods for highly efficient optimisation of geometrically shaped constellations to maximise data throughput in optical communications. It describes methods to analytically calculate the information-theoretical loss and the gradient of this loss as a function of the input constellation shape. The gradients of the mutual information (MI) and generalised mutual information (GMI) are critical to the optimisation of geometrically-shaped constellations. The analytically derived gradients of the achievable information rate metrics with respect to the input constellation are presented. The proposed method allows for improved design of higher cardinality and higher-dimensional constellations for optimising both linear and nonlinear fibre transmission throughput. Near-capacity achieving constellations with up to 8192 points for both 2 and 4 dimensions are presented. In the best case, a GMI value within 0.06 bit/2Dsymbol of the additive white Gaussian noise channel (AWGN) capacity was achieved. Additionally, a design algorithm reducing the design computation time from days to minutes is introduced, allowing for the design of optimised constellations for both linear AWGN and nonlinear fibre channels over a wide range of signal-to-noise ratio values.**

I. Introduction

There is renewed interest in the use of capacity-approaching constellation shaping to further increase the throughput and reach of optical fibre communication systems while providing finer granularity flexible rates. Constellation shaping can be divided into two flavours: probabilistic shaping (PS) and geometrical shaping (GS). In PS, the constellation points are transmitted with unequal probabilities in order to maximise the mutual information (MI) in a given channel, while in GS we keep the constellation probabilities uniform and instead change the position of the equiprobable constellation points.

Recently, constellation shaping has contributed to the increase of the system information spectral density in optical fibre communication systems, where the constellations were designed for the linear additive white Gaussian noise (AWGN) channel. There have been noteworthy results achieved employing constellation shaping in the optical fibre channel using PS [1, 2], GS [3–5] and hybrid combinations of both PS and GS [6]. To maximise the benefits from shaping, the cardinality can be increased to have a greater impact on system performance. When the optimum is not known, the numerical optimisation of the constellation shape to maximise the information rate in a given channel becomes rapidly infeasible as constellation size and dimensionality increase. Larger constellations allow for more degrees of freedom when shaping a constellation for the channel, but that comes at the expense of increased computational complexity. To address this, machine learning has been moderately successful in the design of GS constellations [7–9], to minimise information-theoretical loss, and maximise potential data throughput. In these papers, the machine learning framework is used to obtain an objective function for the increase of performance of the constellation being designed, for which a gradient descent strategy is then employed.

Multiple approaches have been considered. Amongst them is a gradient descent for method the design of tailored probability mass functions for PS constellations for fibre nonlinearity tolerance [10–13]. Similarly, GS constellations have been designed for fibre nonlinearity [14–16] or laser phase noise tolerance [17]. However, in general, the optimum geometric constellation shape for such a channel is still not known.

In the case of GS constellation design, the complexity dramatically increases with constellation order. Both the evaluation of the MI function and the calculation of the gradient function scale poorly with the number of constellation points, making the optimisation of multi-dimensional and/or high-order constellations prohibitively time-consuming. A contributing factor in this is the requirement to compute the gradient of the MI or generalised mutual information (GMI) using exploratory steps, i.e., one MI or GMI calculation for each constellation point; an already costly calculation whose complexity scales rapidly with the number of constellation points. Recent works have proposed the use of orthant symmetry [16], where only a limited subset of the constellation points are optimised in a single orthant, and the remainder are formed as reflections in the other orthants. Although this method greatly simplifies the problem, the design of a constellation within a single orthant still requires a computationally expensive step for every constellation point within the orthant and, therefore, will ultimately severely constrain the maximum order of the constellations that can be designed.

This paper presents a method to analytically calculate the information-theoretical loss and the gradient of this loss as a function of the input constellation shape. The gradients of the

This work was supported in part by a UK EPSRC programme under Grant TransNet EP/R035342/1. The work of G. Liga has received funding by the EuroTechPostdoc programme under the European Union's Horizon 2020 research and innovation programme (Marie Skłodowska-Curie grant agreement No. 754462).

E. Sillekens, P. Bayvel and R.I. Killey are with the Optical Networks Group, the E&EE Department, UCL (University College London), London, UK.

D. Lavery was with the Optical Networks Group, Department of Electronic and Electrical Engineering, University College London, London WC1E 7JE, U.K., and is now with Infinera Canada Inc., Ottawa, ON, Canada. (e-mail: dlavery@ieee.org).

G. Liga is the Electrical Engineering Department, TU/e (Eindhoven University of Technology), Eindhoven, The Netherlands

© 2022 IEEE. Personal use is permitted, but republication/redistribution requires IEEE permission. See https://www.ieee.org/publications/rights/index.html for more information.
Authorized licensed use limited to: University College London. Downloaded on August 17,2022 at 14:04:44 UTC from IEEE Xplore. Restrictions apply.

This article has been accepted for publication in IEEE/OSA Journal of Lightwave Technology. This is the author's version which has not been fully edited and content may change prior to final publication. Citation information: DOI 10.1109/JLT.2022.3197366

MI and GMI are critical to the optimisation of geometrically-shaped constellations. In the process of numerical optimisation, the gradient provides a direction in which to increase or decrease the objective function. While the resulting constellations are not guaranteed to be optimal, significant improvements can be obtained.

Usually, the gradients are calculated using a finite difference method, where for every constellation point the cost function is re-evaluated with a small but finite difference to estimate the partial derivative. However, this method scales poorly with an increasing number of constellation points, resulting in an infeasibly complex task for large cardinality constellations, e.g., constellations with more than 1024 points. A more efficient method is to use automatic differentiation [18, 19]. Automatic differentiation offers faster numerical gradient calculation than the finite difference methods, albeit in general not as fast as calculating the gradient analytically. In this paper, the loss gradient is calculated analytically, an approach that has only been used for bit-error rate (BER) [20] and has, to date, never been applied in optical communications and never used for GMI. Using the analytical expressions for these gradients speeds up the optimisation process by a factor corresponding to the constellation cardinality, i.e., only one calculation is needed for the whole constellation instead of a calculation for each constellation point separately, and is, therefore, an invaluable method for constellation design.

The remainder of the paper is organised as follows. In Section II, the optimisation problem is introduced and, in Section II-D, the optimisation method used in this work is shown. In Section III, an efficient gradient calculation in introduced. Then, in Section IV, the gradient is extended to account for the nonlinearity of the fibre channel. After which, in Sections V and VI, we present results obtained using the algorithms shown in this work for the AWGN channel and the nonlinear fibre channel, respectively, with the conclusions in Section VIII.

II. Preliminaries

This section consists of four subsections: the first introduces the notation used throughout the paper; the second describes the channels used; the third describes the achievable information rates used in the paper for quantifying the performance of the designed constellations. Finally, the fourth describes the optimisation algorithm based on gradients for nonlinear optimisation problems.

A. Notation

In this work, we use the following notation. Let $\mathbb{R}$ and $\mathbb{C}$ denote the real and complex numbers respectively. For random variables we use uppercase letters, e.g., X. We use lowercase letters (e.g. x) and underlined lowercase letters (e.g. $\underline{x}$) for ordinary scalar and vector variables, respectively. Matrices are denoted by boldface letters, e.g. $\boldsymbol{x}$ or $\boldsymbol{I}$. In particular, the matrix containing the M possible constellation symbols coordinates is denoted as $\boldsymbol{x} = [\underline{x}_1, \ldots, \underline{x}_M]^T$ where the constellation symbol $\underline{x_i} = [x_{i,1}, x_{i,2}, \ldots, x_{i,2N}]$ represents the location of the i-th point in $2N$ real dimensions, where N represents the number of phase and amplitude pairs. To denote a set we use a calligraphic letter, $\mathcal{J} = \{1, \ldots, M\}$ is the set of all M indices and $\widetilde{\mathcal{J}_n} = \mathcal{J} \setminus \{n\} = \{j \in \mathcal{J}; j \neq n\}$ is the set of all indices excluding n. To denote a subset of constellation points we use the boldface subscripted notation $\boldsymbol{x}_{\mathcal{S}} = [\underline{x}_{i_1}, \ldots, \underline{x}_{i_Q}]^T$ where $\mathcal{S} = \{i_1, \ldots, i_Q\}$ is the set of indices selecting the constellation symbols. Let $||\boldsymbol{x}||_F = \sqrt{\sum_{i=1}^{M} \sum_{j=1}^{2N} ||x_{i,j}||^2}$ be the Frobenius norm of matrix $\boldsymbol{x} \triangleq \{x_{i,j}\}$ [21, p. 55]. For the probability density functions (pdfs), the conventional notation is used, where, for instance, $f_X(\underline{x})$ denotes the pdf of the random variable X and $f_{Y|Y}(\underline{y}|\underline{x})$ denotes the conditional pdf of the random variable Y given X. Let $|\cdot|$ be the absolute value of a scalar. Let $||\cdot||^2$ and $\langle \cdot, \cdot \rangle$ be the squared vector norm and inner product respectively. Let $(\cdot)^H$ be the conjugate transpose, also known as the Hermitian transpose.

The paper uses matrix calculus, meaning that partial derivatives of a multivariate function are organised in a Jacobian matrix or tensor. Let $\boldsymbol{f}(\boldsymbol{x}) : \mathbb{R}^{M \times 2N} \to \mathbb{R}^{N \times 2N}$ be a function that maps matrix $\boldsymbol{x}$ to another matrix. For this function, the Jacobian in tensor form is defined as:

$$\boldsymbol{J}_{\boldsymbol{f}}(\boldsymbol{x}) = \begin{bmatrix} \dfrac{\partial \boldsymbol{f}}{\partial \underline{x}_1} & \cdots & \dfrac{\partial \boldsymbol{f}}{\partial \underline{x}_n} \end{bmatrix} \tag{1}$$

$$(\boldsymbol{J}_{\boldsymbol{f}}(\boldsymbol{x}))_{i,j,k,l} = \frac{\partial f_{i,j}}{\partial x_{k,l}} \tag{2}$$

where $\dfrac{\partial f_{i,j}}{\partial x_{k,l}}$ is the partial derivative of the i,j-th output to the k,l-th input.

When function $f(\underline{x}) : \mathbb{R}^M \to \mathbb{R}$ maps to a real scalar, then the gradient is defined as $\nabla f(\underline{x}) = \boldsymbol{J}_{\underline{f}}^H(\underline{x})$. Let $(\underline{f} \circ \underline{g})(\underline{x}) = \underline{f}(\underline{g}(\underline{x}))$ be a composition of two functions $\underline{f}(\underline{x})$ and $\underline{g}(\underline{x})$. Then, the Jacobian is defined as $\boldsymbol{J}_{\underline{f} \circ \underline{g}}(\underline{x}) = \boldsymbol{J}_{\underline{f}}(\underline{g}(\underline{x}))\boldsymbol{J}_{\underline{g}}(\underline{x})$. If function $\underline{g}(\underline{x})$ maps a vector to a vector, the Jacobian is a matrix. If the function maps a matrix to a matrix, the Jacobian is a tensor.

B. Channel Models

In this paper, we study the optimisation of MI and GMI in two different channels: i) an AWGN channel, and ii) a discrete-time optical fibre channel. The AWGN channel is modelled as

$$f_{Y|X}(\underline{y}|\underline{x}) = \frac{1}{(\pi\sigma_z^2)^N} \exp\left(\frac{-||\underline{y} - \underline{x}||^2}{\sigma_z^2}\right) \tag{3}$$

with noise variance σ_z^2 per 2 real dimensions. Variable X denotes the transmitted symbols, Gaussian noise is added and then variable Y denotes the received symbols; $\underline{x}$ and $\underline{y}$ are instances of those variables; $f_X(\underline{x})$ and $f_Y(\underline{y})$ are the corresponding probability distribution functions. The transmitted symbols, denoted by the row vector $\underline{x_i}$ of $\boldsymbol{x}$, are uniformly distributed, i.e., $f_X(\underline{x_i}) = 1/M$.

The other channel we consider is the nonlinear fibre channel. The channel is modelled as an AWGN channel whose noise power is dependent on the physical properties of the fibre transmission system, optical transmitted signal power and the amplified spontaneous emission (ASE) noise power [22, 23]. Additionally, the modulation format used for transmission

© 2022 IEEE. Personal use is permitted, but republication/redistribution requires IEEE permission. See https://www.ieee.org/publications/rights/index.html for more information.
Authorized licensed use limited to: University College London. Downloaded on August 17,2022 at 14:04:44 UTC from IEEE Xplore. Restrictions apply.

This article has been accepted for publication in IEEE/OSA Journal of Lightwave Technology. This is the author's version which has not been fully edited and content may change prior to final publication. Citation information: DOI 10.1109/JLT.2022.3197366

impacts the noise power, following [24, 25], and the signal-to-noise ratio (SNR) of an optical fibre channel at optimum launch power can be predicted as

$$\mathrm{SNR} = \frac{P}{P_{\mathrm{ASE}} + \eta_{\mathrm{tot}} P^3} \tag{4}$$

$$\eta_{\mathrm{tot}} P^3 \approx \left(\eta_1 + \eta_2 \Phi(X)\right) P^3 \tag{5}$$

$$\mathrm{SNR}_{\mathrm{opt}} \approx \frac{\left(\frac{\frac{1}{2\eta_1} P_{\mathrm{ASE}}}{(1+\frac{\eta_2}{\eta_1}\Phi(X))}\right)^{\frac{1}{3}}}{P_{\mathrm{ASE}} + \frac{P_{\mathrm{ASE}}}{2}}, \tag{6}$$

with the nonlinear coefficients η_1 and η_2, the launch power P, ASE noise power P_{ASE} and the excess kurtosis $\Phi(X) \triangleq \frac{\mathbb{E}\left[|X|^4\right]}{\mathbb{E}[|X|^2]^2} - 2$ of the complex constellation. A closed form equation for η_1 can be found in [26, Eq. (5,10,11)] and η_2 can be found in [27, Eq. (16)].

To simplify the expression for the performance of a optical transmission system given a transmitted constellation, the dependence on ASE noise power cancels out when describing the expression as a ratio of the optimum SNR of the input distribution and a reference distribution. Effectively lumping the channel description into two terms. Although any reference distribution can be chosen, the Gaussian distribution has zero excess kurtosis, i.e., $\Phi\left(X_{\mathrm{Gaussian}}\right) = 0$, and simplifies the expression even further. The ratio between the optimum SNR for the input distribution X and the reference distribution X_{ref} is then given as

$$\frac{\mathrm{SNR}_{\mathrm{opt}}}{\mathrm{SNR}_{\mathrm{opt,ref}}} = \frac{\left(1 + c\Phi(X)\right)^{-\frac{1}{3}}}{\left(1 + c\Phi(X_{\mathrm{ref}})\right)^{-\frac{1}{3}}} \tag{7}$$

$$\mathrm{SNR}_{\mathrm{opt}} = \left(1 + c\Phi(X)\right)^{-\frac{1}{3}} \mathrm{SNR}_{\mathrm{opt,Gaussian}}\,, \tag{8}$$

with $\mathrm{SNR}_{\mathrm{opt,Gaussian}} = \frac{\left(\frac{1}{2\eta_1} P_{\mathrm{ASE}}\right)^{\frac{1}{3}}}{\frac{3}{2} P_{\mathrm{ASE}}}$ and eta-ratio $c = \frac{\eta_2}{\eta_1}$. Eq. (8) is used to predict the change in SNR when constellation X is used compared to a reference constellation. This means, the channel performance as a function of the constellation is fully described with only $\mathrm{SNR}_{\mathrm{opt,ref}}$, $\Phi(X_{\mathrm{ref}})$ and c. This expression will be used in Sec. IV-B to modify the signal power, effectively changing the SNR as a function of the constellation. Note that, if the modulation format changes, the launch power also changes to the optimum launch power for the new constellation and the other channel parameters remain the same; Eq. (8) can be used to calculate the change in effective SNR. Therefore, the behaviour of the constellations designed for this channel is given by this compact expression, describing the channel with only the eta-ratio c and the SNR at optimum launch power when a reference distribution is transmitted.

C. Achievable Information Rates

In this work, the amount of information that can be reliably transmitted is quantified using achievable information rates (AIRs), specifically MI or GMI. The MI [28], defined between X and Y is given as as [29, Eq. (8.47)]

$$I(X;Y) = \mathop{\mathbb{E}}_{X,Y}\left[\log_2\left(\frac{f_{X,Y}(\underline{x},\underline{y})}{f_X(\underline{x}) f_Y(\underline{y})}\right)\right]. \tag{9}$$

For transmitting and receiving symbols, the MI gives the maximum amount of information, measured in bits per symbol, that we can decode reliably.

In the case of a bit interleaved coded modulation (BICM) scheme, the GMI is a more appropriate measure as it predicts the performance of forward error correction (FEC) schemes [30]. To calculate the GMI, the sum of the mutual information between the input bits C_k and received symbols Y is used. Let $m = \log_2(M)$ be the number of bits transmitted per symbol, a vector of m bits $\underline{c}_i = [c_{i,1}, \ldots, c_{i,m}]^T$ is mapped to a corresponding symbol $\underline{x}_i$. The GMI is given as [31]

$$\begin{aligned} G &= \sum_{k=1}^{m} I(C_k; Y) \\ &= \sum_{k=1}^{m} \mathop{\mathbb{E}}_{C_k,Y}\left[\log_2 \frac{f_{Y|C_k}(\underline{y}|c_k)}{f_Y(\underline{y})}\right]. \end{aligned} \tag{10}$$

An AIR when using a given FEC scheme as inner code can be computed as

$$R^* = mR\left(1 - H_{\mathrm{b}}\big(\mathrm{BER}\big)\right), \tag{11}$$

where m is the number of transmitted bits per 2D, R the inner FEC code rate and $\big(1 - H_{\mathrm{b}}(p)\big) = 1 + p\log_2 p + (1-p)\log_2(1-p)$ is the capacity of the binary symmetric channel with cross-over probability p determined by the binary input of the FEC encoder and the binary output of the FEC decoder. The decoder output is here assumed to contain independent errors after the use of an ideal interleaver. The BER is obtained with error counting after the soft-decision FEC decoder. In the remainder of this paper, this rate is used as a performance metric, together with MI and GMI.

We use MI and GMI to refer to the quantities defined in Eq. (9) and Eq. (10), respectively. The generic AIR label is used whenever different information rates are shown (including MI, GMI and R^*).

D. Nonlinear Optimisation Methods Based on Gradients

For the optimisation problem, i.e., finding the locations of constellation points that maximise throughput, we used a gradient descent algorithm. Optimising the constellations for GMI is a nonconvex problem and therefore the optimsation is affected by converging to a non-global minima. Although for nonconvex problems the derivative driven algorithms are not guaranteed to converge to global optima, we have have obtained good results. We have compared both acBFGS [32–35] and trust-region optimisation algorithm and observed fewer local minima from the trust-region. In this work,we focused on the trust-region algorithms [36–38] where the Jacobian of the Jacobian, known as the Hessian, is estimated using a symmetric rank-one method [39] as described in [40, p. 146]. The optimisation step is described by

$$\underline{x}_{k+1} = \underline{x}_k + \underline{s}_k\,, \tag{12}$$

© 2022 IEEE. Personal use is permitted, but republication/redistribution requires IEEE permission. See https://www.ieee.org/publications/rights/index.html for more information.
Authorized licensed use limited to: University College London. Downloaded on August 17,2022 at 14:04:44 UTC from IEEE Xplore. Restrictions apply.

This article has been accepted for publication in IEEE/OSA Journal of Lightwave Technology. This is the author's version which has not been fully edited and content may change prior to final publication. Citation information: DOI 10.1109/JLT.2022.3197366

where $\underline{x}_k$ is the constellation at step k and the update $\underline{s}_k$ is determined by the trust-region sub-problem defined as

$$\min_{\underline{s}_k} f_k + \underline{g}_k^T \underline{s}_k + \frac{1}{2}\underline{s}_k^T \boldsymbol{B}_k \underline{s}_k \quad \text{s.t. } ||\underline{s}_k|| \leq \Delta_k \,, \tag{13}$$

where f_k is the function value, $\underline{g}_k$ is the gradient and $\boldsymbol{B}_k$ the inverse of the Hessian at $\underline{x}_k$. The trust region Δ_k limits the size of the step $\underline{s}_k$ which shrinks as we get close to optimum by the algorithm. We initialise this parameter of the algorithm as 1. For this method, we need an accurate gradient as it is used for both the step and the Hessian estimation. The next step is to solve the step sub-problem Eq. (13), for which we use Steihaug's conjugate gradient method [41]. The sub-problem is a simpler problem and easier to optimise than the entire optimisation problem and the sub-problem is solved at every step. Finding a solution for the sub-problem is often less computationally expensive than a single gradient calculation of the AIR with respect to the input constellation. A fast trust-region optimisation algorithm is possible via the improvements proposed in Sec. III, where we describe the efficient gradient calculation proposed in this work.

III. Efficient Gradient Computation of MI and GMI for the AWGN Channel

One of the difficulties of calculating the gradients of MI and GMI is that, for a fixed AWGN variance, the input constellation needs to be constrained to constant average power. The most straightforward approach to constellation optimisation is to use the finite-difference method, renormalising the constellation after every finite-difference exploration step for the gradient calculation. However, the renormalisation has the consequence that, without extra manipulation, the entire objective function needs to be recalculated, for every constellation point, for every dimension. This is because, if the location of a single constellation point is changed, all the points need to be rescaled to maintain the same average power.

In this work, we propose an efficient method of obtaining the gradient by splitting the problem into two functions in a composition. The first function normalises the constellation — that is, it takes the constellation points as an input and outputs a vector of normalised constellation points. The output of the first function is then passed to a function that is either an unconstrained MI or GMI function. This maps a vector with all constellation points to a single AIR value, in this work we use Eq. (9) and Eq. (10).

Additionally, after some algebraic transformation of the complete objective function, the gradient can be expressed as a rearrangement of the terms used to calculate the MI and GMI. The integral calculating the expectation of the Gaussian-noise variable still needs to be evaluated, which can be done efficiently using a Gauss-Hermite quadrature (GHQ) [31].

A. Mutual Information (MI)

We start by analysing the MI calculation for the AWGN channel. The MI and GMI calculations as presented in this work are similar and the derivation for the simpler MI calculation can be taken over to the GMI derivation. Let the MI function be [31, Eq. (21)]

$$I = m - \frac{1}{M}\sum_{i=1}^{M} \int_{\mathbb{R}^{2N}} f(\underline{z}) g_i(\underline{z}, \boldsymbol{x}_{\mathcal{J}}) \mathrm{d}\underline{z} \,, \tag{14}$$

where

$$f(\underline{z}) = \frac{1}{(\pi\sigma_z^2)^N} \exp\left(\frac{||\underline{z}||^2}{-\sigma_z^2}\right) \tag{15}$$

$$g_i(\underline{z}, \boldsymbol{x}_{\mathcal{J}}) \triangleq \log_2\left(\sum_{j\in\mathcal{J}} h(\underline{z}, \underline{x}_i, \underline{x}_j)\right) \tag{16}$$

$$h(\underline{z}, \underline{x}_i, \underline{x}_j) \triangleq \exp\left(\frac{||\underline{x}_i - \underline{x}_j||^2 + 2\langle \underline{z}, (\underline{x}_i - \underline{x}_j)\rangle}{-\sigma_z^2}\right) , \tag{17}$$

with $\mathcal{J} = \{1, \ldots, M\}$, $\underline{z} = \underline{y} - \underline{x}_i$, $\underline{d}_{ij} = -\underline{d}_{ji} = \underline{x}_i - \underline{x}_j$ and σ_z^2 the noise variance per 2 real dimensions. The variable Z is a substitution to split the additive noise from the transmitted symbol for the expected value calculation.

Following the steps in Appendix A, we obtain:

$$\nabla I = [\frac{\partial}{\partial \underline{x}_1} I, \frac{\partial}{\partial \underline{x}_2} I, \ldots, \frac{\partial}{\partial \underline{x}_M} I], \tag{18}$$

where

$$\frac{\partial}{\partial \underline{x}_n} I = -\frac{1}{M}\int_{\mathbb{R}^{2N}} f(\underline{z}) \left[\frac{\sum_{j\in\widetilde{\mathcal{J}_n}} \left(\frac{2\underline{d}_{nj}+2\underline{z}}{-\sigma_z^2}\right) h(\underline{z}, \underline{x}_n, \underline{x}_j)}{\log(2)\sum_{j\in\mathcal{J}} h(\underline{z}, \underline{x}_n, \underline{x}_j)} + \sum_{i\in\widetilde{\mathcal{J}_n}} \frac{-\left(\frac{2\underline{d}_{in}+2\underline{z}}{-\sigma_z^2}\right) h(\underline{z}, \underline{x}_i, \underline{x}_n)}{\log(2)\sum_{j\in\mathcal{J}} h(\underline{z}, \underline{x}_i, \underline{x}_j)} \right] \mathrm{d}\underline{z} \,, \tag{19}$$

and $\widetilde{\mathcal{J}_n} = \mathcal{J} \setminus \{n\} = \{j \in \mathcal{J}; j \neq n\}$.

We can simplify the computation of Eq. (19) by using the symmetry in $\underline{z}$ and $\underline{d}_{ij}$

$$\frac{\partial}{\partial \underline{x}_n} g_i(\underline{z}, \boldsymbol{x}_{\mathcal{J}}) = \frac{\partial}{\partial \underline{x}_i} g_n(\underline{z}, \boldsymbol{x}_{\mathcal{J}}) \,. \tag{20}$$

To calculate the gradient using Eq. (19), we only need M^2 of the subfunction Eq. (17), all of which is already calculated for the MI calculation. For the finite-differences approach, at least $2N \times M$ more are needed.

Then, to obtain the gradient we need to calculate the multidimensional integral over the support of $\underline{z}$ in Eq. (19). To compute the MI and its gradient in the AWGN channel, we can use the GHQ to efficiently numerically evaluate the integral [31, Sec. IV.B].

B. Generalised Mutual Information (GMI)

For the bit-wise decoder commonly used in BICM channels, the GMI is an accurate predictor of the post-FEC performance. To optimise the GMI [31, Eq. (22)], we compute its gradient

© 2022 IEEE. Personal use is permitted, but republication/redistribution requires IEEE permission. See https://www.ieee.org/publications/rights/index.html for more information.
Authorized licensed use limited to: University College London. Downloaded on August 17,2022 at 14:04:44 UTC from IEEE Xplore. Restrictions apply.

This article has been accepted for publication in IEEE/OSA Journal of Lightwave Technology. This is the author's version which has not been fully edited and content may change prior to final publication. Citation information: DOI 10.1109/JLT.2022.3197366

similarly to what done for Eq. (19). We then start from expanding Eq. (10) to

$$G = m - \frac{1}{M} \sum_{b\in\{0,1\}} \sum_{i\in\mathcal{I}_k^b} \sum_{k=1}^{m} \int_{\mathbb{R}^{2N}} f(\underline{z}) \log_2 \left(\frac{\sum_{j\in\mathcal{J}} h(\underline{z},\underline{x}_i,\underline{x}_j)}{\sum_{p\in\mathcal{I}_k^b} h(\underline{z},\underline{x}_i,\underline{x}_p)} \right) \mathrm{d}\underline{z}\,, \quad (21)$$

where $\mathcal{I}_k^b = \{i \in \mathcal{J}; c_{i,k} = b\}$ is the set of indices where the k-th bit is b.

Eq. (21) can be rewritten to be more similar to Eq. (14) and derive a gradient similarly to Eq. (19):

$$G = m - \frac{1}{M} \sum_{b\in\{0,1\}} \sum_{i\in\mathcal{I}_k^b} \sum_{k=1}^{m} \int_{\mathbb{R}^{2N}} f(\underline{z}) \left[\log_2 \left(\sum_{j\in\mathcal{J}} h(\underline{z},\underline{x}_i,\underline{x}_j) \right) - \log_2 \left(\sum_{p\in\mathcal{I}_k^b} h(\underline{z},\underline{x}_i,\underline{x}_p) \right) \right] \mathrm{d}\underline{z}\,. \quad (22)$$

Now after introducing a new subfunction where the sum is dependent on the bit mapping, $\mathcal{I}_k^b$,:

$$g_i(\underline{z}, \boldsymbol{x}_{\mathcal{I}_k^b}) \triangleq \log_2 \left(\sum_{p\in\mathcal{I}_k^b} h(\underline{z},\underline{x}_i,\underline{x}_p) \right)\,, \quad (23)$$

for which the partial derivative can be calculated equivalently to Appendix A, Eq. (48), we can formulate the gradient for the GMI as

$$\begin{aligned} \frac{\partial}{\partial x_n} G = &-\frac{-m}{M} \int_{\mathbb{R}^{2N}} f(\underline{z}) \frac{\partial}{\partial \underline{x}_n} g_i(\underline{z}, \boldsymbol{x}_{\mathcal{J}}) \mathrm{d}\underline{z} \\ &-\frac{m}{M} \sum_{i\in\widetilde{\mathcal{J}}_n} \int_{\mathbb{R}^{2N}} f(\underline{z}) \frac{\partial}{\partial \underline{x}_{n\in J}} g_i(\underline{z}, \boldsymbol{x}_{\mathcal{J}}) \mathrm{d}\underline{z} \\ &-\frac{1}{M} \sum_{k=1}^{m} \int_{\mathbb{R}^{2N}} f(\underline{z}) \frac{\partial}{\partial \underline{x}_n} g_i(\underline{z}, \boldsymbol{x}_{\mathcal{I}_k^b}) \mathrm{d}\underline{z} \\ &-\frac{1}{M} \sum_{k=1}^{m} \sum_{i\in\widetilde{\mathcal{I}}_{nk}^b} \int_{\mathbb{R}^{2N}} f(\underline{z}) \frac{\partial}{\partial \underline{x}_{n\in J}} g_i(\underline{z}, \boldsymbol{x}_{\mathcal{I}_k^b}) \mathrm{d}\underline{z} \end{aligned}\,, \quad (24)$$

where $\widetilde{\mathcal{I}}_{nk}^b = \{i \in \mathcal{I}_k^b; i \neq n\}$.

Following the steps from Sec. III-A, the gradient of the GMI is:

$$\nabla G = [\frac{\partial}{\partial \underline{x}_1} G, \frac{\partial}{\partial \underline{x}_2} G, \ldots, \frac{\partial}{\partial \underline{x}_M} G] \quad (25)$$

$$\begin{aligned} \frac{\partial}{\partial \underline{x}_n} G = -\frac{1}{M} \int_{\mathbb{R}^{2N}} f(\underline{z}) \Bigg[& m \frac{\sum_{j\in\widetilde{\mathcal{J}}_n} \left(\frac{2\underline{d}_{nj}+2\underline{z}}{-\sigma_z^2} \right) h(\underline{z},\underline{x}_n,\underline{x}_j)}{\log(2) \sum_{j\in\mathcal{J}} h(\underline{z},\underline{x}_n,\underline{x}_j)} \\ & + m \sum_{i\in\widetilde{\mathcal{J}}_n} \frac{-\left(\frac{2\underline{d}_{in}+2\underline{z}}{-\sigma_z^2} \right) h(\underline{z},\underline{x}_i,\underline{x}_n)}{\log(2) \sum_{j\in\mathcal{J}} h(\underline{z},\underline{x}_i,\underline{x}_j)} \\ & + \sum_{k=1}^{m} \frac{\sum_{j\in\widetilde{\mathcal{I}}_{nk}^b} \left(\frac{2\underline{d}_{nj}+2\underline{z}}{-\sigma_z^2} \right) h(\underline{z},\underline{x}_n,\underline{x}_j)}{\log(2) \sum_{j\in\mathcal{J}} h(\underline{z},\underline{x}_n,\underline{x}_j)} \\ & + \sum_{k=1}^{m} \sum_{i\in\widetilde{\mathcal{I}}_{nk}^b} \frac{-\left(\frac{2\underline{d}_{in}+2\underline{z}}{-\sigma_z^2} \right) h(\underline{z},\underline{x}_i,\underline{x}_n)}{\log(2) \sum_{j\in\mathcal{J}} h(\underline{z},\underline{x}_i,\underline{x}_j)} \Bigg] \mathrm{d}\underline{z}\,. \end{aligned} \quad (26)$$

Now, again, the only step left to obtain the gradient is to evaluate the expected value of the multidimensional integral over the support of $\underline{z}$, which again can be numerically evaluated with a GHQ.

IV. Channel Specific Constellation Optimisation

In the previous section, we simply computed the gradient of the MI and GMI for the AWGN channel. This allows us to compute the performance metric given the constellation coordinates and fixed noise variance. For optimisation of constellations in the AWGN channel, the SNR is fixed at the desired value. When looking at the definition of SNR $\triangleq \frac{\mathrm{E}[||X||^2]}{\mathrm{E}[||Z||^2]}$, and assuming that the $\mathrm{E}[||Z||^2] \triangleq N\sigma_z^2$ is fixed, it can be seen that the signal power $\mathrm{E}[||X||^2]$ needs to be constrained, as previously noted. Normalising the constellation leads to an unconstrained optimisation problem which is invariant to the input constellation energy. This invariance is achieved by introducing a normalisation function and defining the optimisation function as the composite of the normalisation and the AIR, as described in the next section.

A. Gradient chain rule for the AWGN Channel

For the AWGN channel, the only extra function we need to introduce is the normalisation function. We can define a normalisation function as

$$\boldsymbol{u}(\boldsymbol{x}) = \frac{\boldsymbol{x}}{\sqrt{\frac{1}{MN}||\boldsymbol{x}||_F}}\,, \quad (27)$$

whose Jacobian is given by

$$\boldsymbol{J}_{\underline{u}} = \frac{||\boldsymbol{x}||_F^2 \mathbf{I}_{M,2N} - \boldsymbol{x}\otimes\boldsymbol{x}}{\sqrt{\frac{1}{MN}||\boldsymbol{x}||_F^3}} \quad (28)$$

$$(\mathbf{I}_{M,2N})_{i,j,k,l} = \begin{cases} 1 & \text{if } i=j \wedge k=l \\ 0 & \text{otherwise} \end{cases} \quad (29)$$

$$(\boldsymbol{x}\otimes\boldsymbol{x})_{i,j,k,l} = \underline{x}_{i,j}\underline{x}_{k,l}\,, \quad (30)$$

for the complex $M \times 2N$ vector $\underline{x} \in \mathbb{R}^{M\times 2N}$ and $\boldsymbol{J}, \boldsymbol{I} \in \mathbb{R}^{M,D,M,2N}$. With this function and its Jacobian, we can use

© 2022 IEEE. Personal use is permitted, but republication/redistribution requires IEEE permission. See https://www.ieee.org/publications/rights/index.html for more information.
Authorized licensed use limited to: University College London. Downloaded on August 17,2022 at 14:04:44 UTC from IEEE Xplore. Restrictions apply.

This article has been accepted for publication in IEEE/OSA Journal of Lightwave Technology. This is the author's version which has not been fully edited and content may change prior to final publication. Citation information: DOI 10.1109/JLT.2022.3197366

the following objective function and apply the chain rule to obtain the gradient

$$o(\underline{x}) = f\big(\boldsymbol{u}(\underline{x})\big) \tag{31}$$

$$\nabla o(\underline{x}) = (\boldsymbol{J}_o(\underline{x}))^H = \Big(\boldsymbol{J}_f\big(\boldsymbol{u}(\underline{x})\big)\boldsymbol{J}_{\boldsymbol{u}}(\underline{x})\Big)^H, \tag{32}$$

which can be used in the optimisation method. Here, we can use the MI from Eq. (14) as $f(\underline{x})$ and its gradient, i.e., Eq. (18), as $\boldsymbol{J}_f(\underline{x})$.

In summary, for an MI calculation, first the constellation is normalised using Eq. (27). Next, we calculate the contribution to the GMI and the gradient for each constellation point separately. Starting from x_i we pre-calculate

$$h(\underline{z}, \underline{x}_i, \underline{x}_j) = \exp\left(\frac{||\underline{d}_{ij}||^2 + 2\langle \underline{z}, \underline{d}_{ij}\rangle}{-\sigma_z^2}\right) \tag{33}$$

for all x_j and sample points z, n.b., if $x_i = x_j$, the result is 1. The MI is calculated by first summing tributaries $h(\underline{z}, \underline{x}_i, \underline{x}_j)$ over j and then, after taking the log, taking the (weighted) sum over z. For the gradient calculation, start by summing all tributaries of $h(\underline{z}, \underline{x}_i, \underline{x}_j)$ over j, then multiplying by $2(\underline{z} + \underline{d}_{ij})$ and finally take the (weighted) sum over z. Sum the contributions over all i and scale with constants according to the integration method chosen.

B. Gradient chain rule for the Nonlinear Fibre Channel

To extend the method to optimise the constellation for the nonlinear fibre channel, the normalisation function is extended to reflect the change in SNR as a function of the transmitted constellation described in section II-B. When calculating the AIR for the nonlinear fibre channel, the performance of the constellation is evaluated at optimum launch power. Assuming a known SNR for a reference constellation at know launch power, the constellation can be scaled to reflect the SNR change due to the fibre nonlinearity compared to the reference constellation. For convenience, a Gaussian distribution is used as the reference constellation, as shown in Eq. (8). The AIR can then be calculated using either Eq. (14) or Eq. (22) with the scaled constellation as the input. This is performed analogously to the normalisation function Eq. (27) and its effect on the gradient Eq. (31) is described as:

$$o(\boldsymbol{x}) = f(\boldsymbol{n}(\boldsymbol{u}(\boldsymbol{x}))) \tag{34}$$

$$\boldsymbol{n}(\boldsymbol{x}) = \boldsymbol{x}\sqrt{(1 + c\Phi(\boldsymbol{x}))^{-\frac{1}{3}}}, \tag{35}$$

reflecting the amplitude change as described in Eq. (8).

We can now define functions $v(\boldsymbol{x})$ and $w(\boldsymbol{x})$ to calculate its Jacobian of $\boldsymbol{n}(\boldsymbol{x})$:

$$\boldsymbol{n}(\boldsymbol{x}) = \boldsymbol{x}\left(1 + c\left(\frac{v(\boldsymbol{x})}{w(\boldsymbol{x})} - 2\right)\right)^{-\frac{1}{6}} \tag{36}$$

$$v(\boldsymbol{x}) = \frac{1}{M}\sum_{j=1}^{M}\left(\Re\{x_j\}^2 + \Im\{x_j\}^2\right)^2 \tag{37}$$

$$w(\boldsymbol{x}) = \left(\frac{1}{M}\sum_{j=1}^{M}\left(\Re\{x_j\}^2 + \Im\{x_j\}^2\right)\right)^2 \tag{38}$$

for which we can find derivatives

$$v'(\boldsymbol{x}) = \frac{\partial}{\partial x_i}v(\boldsymbol{x}) = \frac{4x_i}{M}\left(\Re\{x_j\}^2 + \Im\{x_j\}^2\right) \tag{39}$$

$$w'(\boldsymbol{x}) = \frac{\partial}{\partial x_i}w(\boldsymbol{x}) = \frac{4x_i}{M}\left(\frac{1}{M}\sum_{j=1}^{M}\left(\Re\{x_j\}^2 + \Im\{x_j\}^2\right)\right). \tag{40}$$

Then, we can obtain the Jacobian in two steps, first the diagonal

$$\begin{aligned}\frac{\partial}{\partial x_i}n_i(\boldsymbol{x}) = &\left(1 + c\left(\frac{v(\boldsymbol{x})}{w(\boldsymbol{x})} - 2\right)\right)^{-\frac{1}{6}} \\ &- \frac{x_i}{6}\left(1 + c\left(\frac{v(\boldsymbol{x})}{w(\boldsymbol{x})} - 2\right)\right)^{-\frac{7}{6}} \\ &\cdot\left(\frac{v'(\boldsymbol{x})w(\boldsymbol{x}) - v(\boldsymbol{x})w'(\boldsymbol{x})}{w(\boldsymbol{x})^2}\right).\end{aligned} \tag{41}$$

Now for all elements not on the diagonal, i.e. $i \neq p$, we obtain:

$$\begin{aligned}\frac{\partial}{\partial x_i}n_p(\boldsymbol{x}) = &-\frac{x_p}{6}\left(1 + c\left(\frac{v(\boldsymbol{x})}{w(\boldsymbol{x})} - 2\right)\right)^{-\frac{7}{6}} \\ &\cdot\left(\frac{v'(\boldsymbol{x})w(\boldsymbol{x}) - v(\boldsymbol{x})w'(\boldsymbol{x})}{w(\boldsymbol{x})^2}\right),\end{aligned} \tag{42}$$

with $|x_j|^2 = \Re\{x_j\}^2 + \Im\{x_j\}^2$ and

$$\begin{aligned}&\frac{v'(\boldsymbol{x})w(\boldsymbol{x}) - v(\boldsymbol{x})w'(\boldsymbol{x})}{w(\boldsymbol{x})^2} \\ &\quad= \frac{4Mx_i\left(|x_i|^2\sum_{j=1}^{M}|x_j|^2 - \sum_{j=1}^{M}|x_j|^4\right)}{\left(\sum_{j=1}^{M}|x_j|^2\right)^3}.\end{aligned} \tag{43}$$

Note that because of the dimensionality of $\boldsymbol{x} \in \mathbb{C}^{M,1}$ each individual symbol x_i is here a complex scalar. To scale the current model beyond a single dimension needs further work [42].

This result can be used to extend Eq. (31) to include the expected change in SNR from reduced nonlinear distortion due to the changed excess kurtosis of the constellation. This new objective function then finds constellations where the trade-off between shaping and nonlinearity is optimised.

V. Results for the AWGN Channel

In this section, the performance of the optimised constellations in the AWGN channel is shown. The optimisation process is described in detail in appendix B. In Fig. 1, an example of a constellation undergoing the optimisation process is shown. The optimisation trajectory for 12 dB SNR using a regular 64-quadrature amplitude modulation (QAM) as a starting constellation is shown. The 64-QAM constellation is chosen for clarity of illustration of the optimisation trajectory, due to its relatively low cardinality. The constellation points generally do not have a linear optimisation trajectory, but the optimisation does result in a regular-looking constellation. For the example constellation, the result resembles an amplitude and phase-shift keyed (APSK) constellation where the inner

© 2022 IEEE. Personal use is permitted, but republication/redistribution requires IEEE permission. See https://www.ieee.org/publications/rights/index.html for more information.
Authorized licensed use limited to: University College London. Downloaded on August 17,2022 at 14:04:44 UTC from IEEE Xplore. Restrictions apply.

This article has been accepted for publication in IEEE/OSA Journal of Lightwave Technology. This is the author's version which has not been fully edited and content may change prior to final publication. Citation information: DOI 10.1109/JLT.2022.3197366

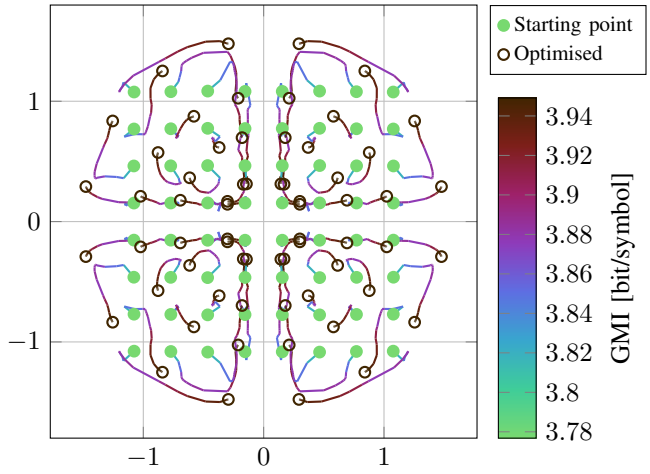

Fig. 1. Optimisation trajectory, starting from a regular 64-QAM, the constellation is optimised for 12 dB SNR and improves 0.17 bit/symbol.

amplitude ring has two constellation points for every value of phase shift.

Next, we describe at the results for 2D and 4D geometrically shaped constellations for the AWGN channel. To obtain these results, we followed the trust-region method of Sec. II-D with the GMI gradient in Eq. (26) and the normalisation for the AWGN channel Eq. (27). The optimisation is carried out by starting with different initial constellations. Two fixed constellations; namely, a regular QAM constellation and one designed following [43], as well as randomly generated starting points. In the optimisation, symmetry around every axis was imposed, akin to the binary reflected Gray code (BRGC), so that the most significant bit describes which half of the plane the constellation point is in and the other half of the points are a mirrored copy. As both the regular QAM and the constellations from Méric [43] already meet these requirements, these constellations can be directly used as a starting point for these optimisations. We have found the solutions with these constraints performed equally well as solutions that allowed asymmetries in the region where the MI/GMI are close to the maximum entropy of the constellations. By using Eq. (31), we can obtain more accurate gradients with fewer iterations. This allows the optimisation of high cardinality constellations, which in this paper were selected to be up to 8192 points.

A. 2D Constellations Shaping for the AWGN Channel

The performance of the geometrically shaped 2-dimensional (GS-2D) constellations tailored to the AWGN channel is shown in Fig. 2 and is illustrated in terms of gap to AWGN capacity at the SNR the constellation is optimised for. The optimisation was performed for $m = 3, 4, ..., 13$, and for integer values of SNR in the range shown. It can be seen that the performance of higher-cardinality constellations in terms of gap to capacity improves compared to the results obtained for lower-order modulation formats.

The capacity of the AWGN channel is $\log_2(1+\mathrm{SNR})$ bit/2D [28]. One would expect the MI and GMI to grow in line with the capacity until the throughput is limited by the cardinality of the constellation. Therefore, before saturation is reached the gap between GMI and the AWGN capacity falls within a relatively small range compared to the achieved GMI. Showing the performance of the optimised constellations as the gap to the AWGN capacity improves the presentation of the results, plotted over a wide range of SNRs.

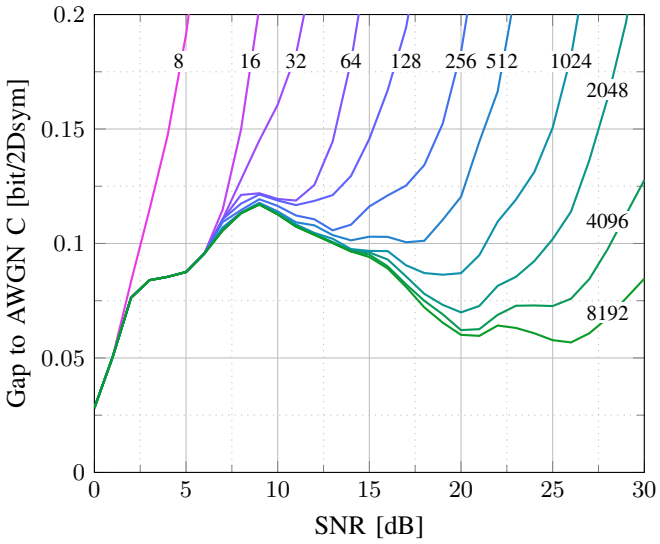

Fig. 2. Gap to capacity in GMI for optimised GS-2D constellations tailored to the AWGN channel enforcing 2 axes of symmetry for every round number SNR. Numbers on the lines indicate the constellation order.

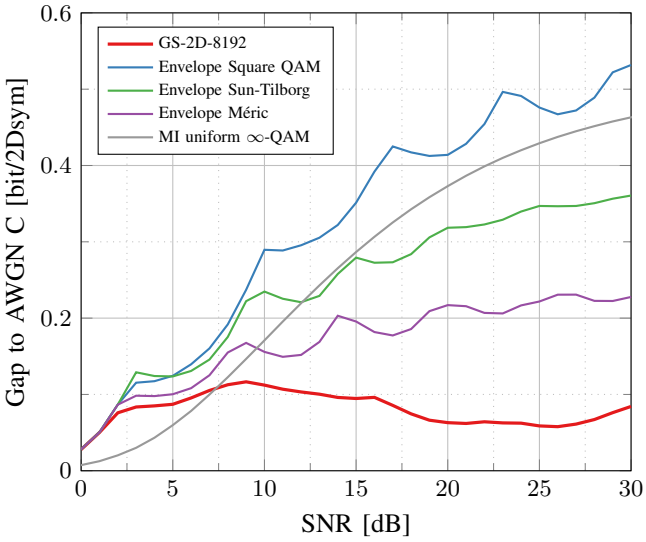

Fig. 3. Gap to capacity in GMI for optimised quadrant-symmetric 8192-ary constellation compared to the envelopes of regular square QAM, Sun-Tilborg [44] and Méric [43]. The MI for uniform ∞-QAM is shown a reference for the 1.53 dB shaping gain [45].

In Fig. 3, the performance of the 2-dimensional optimised constellation is shown for the highest cardinality constellation $M = 8192$ investigated in this work. This performance is compared to the one of benchmark constellations such as square QAM, Sun-Tilborg [44] and Méric constellations [43], the latter two being capacity-approaching in terms of MI. The

© 2022 IEEE. Personal use is permitted, but republication/redistribution requires IEEE permission. See https://www.ieee.org/publications/rights/index.html for more information.
Authorized licensed use limited to: University College London. Downloaded on August 17,2022 at 14:04:44 UTC from IEEE Xplore. Restrictions apply.

This article has been accepted for publication in IEEE/OSA Journal of Lightwave Technology. This is the author's version which has not been fully edited and content may change prior to final publication. Citation information: DOI 10.1109/JLT.2022.3197366

cardinality of the benchmark constellations was varied based on the selected SNR (up to $M = 8192$) and the performance of the resulting envelopes is shown in Fig. 3. The MI for uniform ∞-QAM is shown as a reference and it can be seen that it saturates to the 1.53 dB (0.51 bit) gap [45]. The optimised $M = 8192$ gives the best performance of all cardinalities considered. For the optimisation method presented in this paper, the higher cardinality constellation will always achieve the performance of a lower cardinality constellation by taking the lower cardinality constellation and doubling each constellation point (two constellation points having the same coordinates), effectively ignoring the transmitted bit which selects between two constellation points with identical coordinates. It can be seen that the optimised constellations from this work outperform all other constellations in terms of GMI for all SNR values between 0 and 30 dB. The GMI of our optimal constellation also outperforms the MI of uniform ∞-QAM for SNR >7 dB.

B. 4D Constellations Shaping for the AWGN Channel

The significant improvements in computation efficiency now allow us to extend the optimisation of constellations for the AWGN channel to 4D, something which has been challenging to achieve to date. In Fig. 4, the results of optimising constellations for the 4D AWGN channel are shown. The results follow a similar trend to the results presented for 2D, however, we can see that a cardinality of 8192 is not enough to decrease the gap to capacity for higher SNR values.

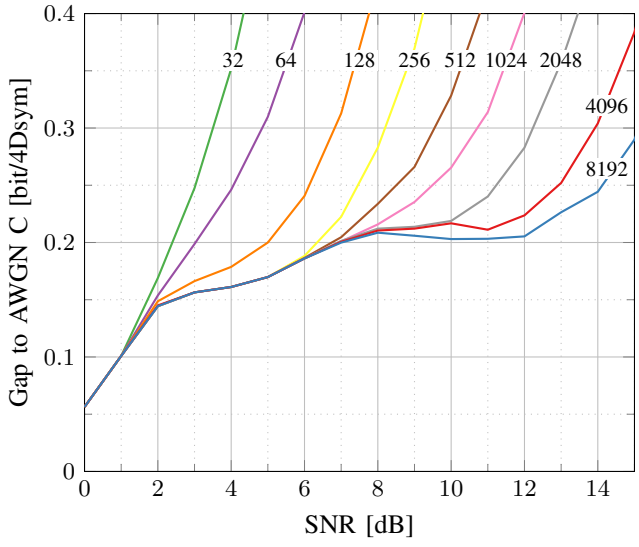

Fig. 4. GMI-capacity gap for optimised GS-4D constellations tailored to the AWGN channel enforcing 4 axes of symmetry for every round number SNR. Numbers on the lines indicate the constellation order M.

Next, we compare the performance of the designed constellations with the recently published 4D constellation with symmetry constraints, presented in [16], which the authors named orthant symmetric (OS). The authors showed how it was possible to reduce the 128-ary constellation to just 5 variables. The 128×4 variables describing all points in all dimensions were reduced to 32 by enforcing symmetry and that subspace was then intuitively spanned using 5 variables. In contrast, the method introduced in this paper greatly improves the efficiency of the constellation design and allows the optimisation of all variables within the orthant. In the case of 128 constellation points this is 32 points with 4 dimensions each, totalling 128 variables.

For this comparison we used the same simulation parameters from [16]; split-step Fourier method (SSFM) simulation [46] of 80-km fibre spans with 100 logarithmically distributed steps, 0.21 dB/km attenuation, chromatic dispersion of 16.9 ps/(nm·km) with a nonlinear coefficient γ of 1.32 /(W·km), amplified with a 4.5 dB noise figure optical amplifier. The transmitted signal consisted of 11 channels of 45 Gbd, spaced at 50 GHz. All transmitted channels had different randomly generated data and only the centre channel was demodulated. A root-raised cosine filter with 1% roll-off was used for matched filtering. The fibre propagation was emulated by using the SSFM with a fixed step size of 100 m. The post-FEC results were obtained using the $R = 4/5$ DVB-S2 low-density parity check (LDPC) decoded with 200 iterations. For each point, the optical launch power was swept in steps of 0.5 dB to find the maximum SNR as a function of distance.

The performance of the resulting geometrically shaped 4-dimensional (GS-4D) constellation is shown in Fig. 5. We can see that the additional freedom from optimising all points in the orthant individually allowed our constellation to outperform the constellation obtained using the approach in [16], albeit by a small margin (0.033 bit/4Dsym) or 120 km; a similar observation to that made by the authors in [16]. The results are shown in terms of both BER and GMI. For the BER a post-FEC curve is shown where the $R = 4/5$ LDPC from [47] is applied.

However, because the optimisation in this work does not rely on higher-order symmetry to reduce the number of optimisation variables and it is significantly more computationally efficient to optimise, we can now optimise constellations with a large number of constellation points. In Fig. 6, the results using the same simulation system for a greater number of constellation points are shown. The orthant symmetry is kept as the lower SNRs does not result in worse performance. The results are shown in terms of both BER and GMI; for the BER a post-FEC curve is shown for a $R = 4/5$ LDPC code from [47]. The performance of the LDPC-coded scheme is shown in terms of R^* from Eq. (11). We can see that for constellations with a number of points ranging from 32 to 8196 in 4 dimensions, we have successfully designed constellations targeting the $R = 4/5$ rate. The R^* saturates at mR for shorter distances until it reaches the GMI. Additionally, the 4096-ary constellation from this optimisation is used in Sec. VI, where it is compared against other constellations with the same number of bits per dimension in Fig. 8.

VI. Results for the Nonlinear Fibre Channel

The results of the shaping of 2D constellations, shaped for the nonlinear fibre channel, as described in Sec. II-B, are shown in Fig. 7. The results shown were calculated using

© 2022 IEEE. Personal use is permitted, but republication/redistribution requires IEEE permission. See https://www.ieee.org/publications/rights/index.html for more information.
Authorized licensed use limited to: University College London. Downloaded on August 17,2022 at 14:04:44 UTC from IEEE Xplore. Restrictions apply.

This article has been accepted for publication in IEEE/OSA Journal of Lightwave Technology. This is the author's version which has not been fully edited and content may change prior to final publication. Citation information: DOI 10.1109/JLT.2022.3197366

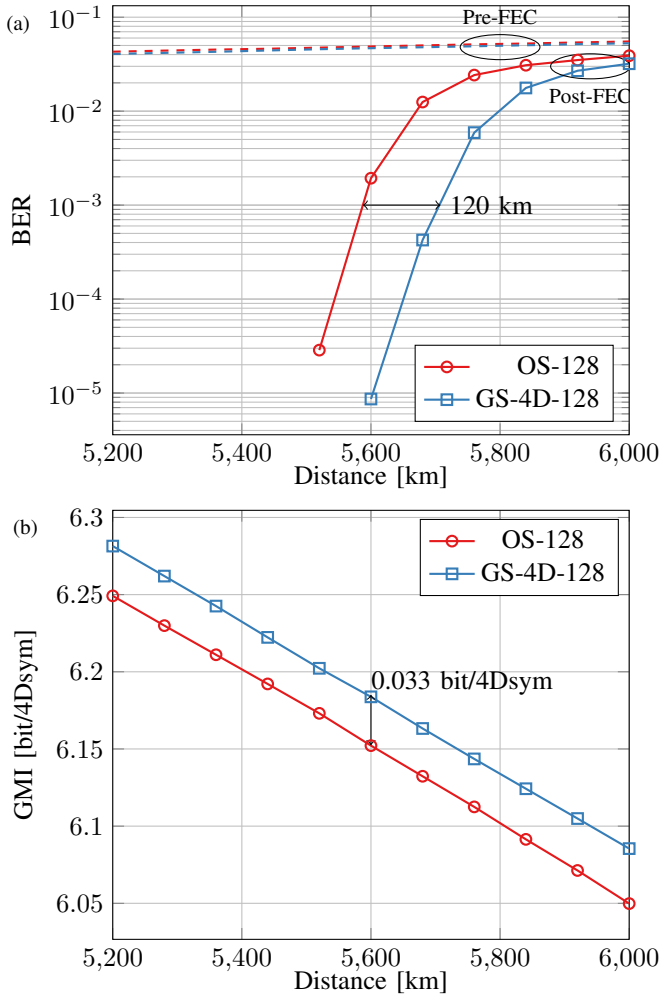

Fig. 5. Comparison between the OS-128 constellation from [16] and a 128-ary constellation designed with the method shown in this work on a simulated fibre system. (a) shows the pre- and post-FEC BER for the $R = 4/5$ DVB-S2 LDPC and (b) shows the GMI vs the transmitted distance.

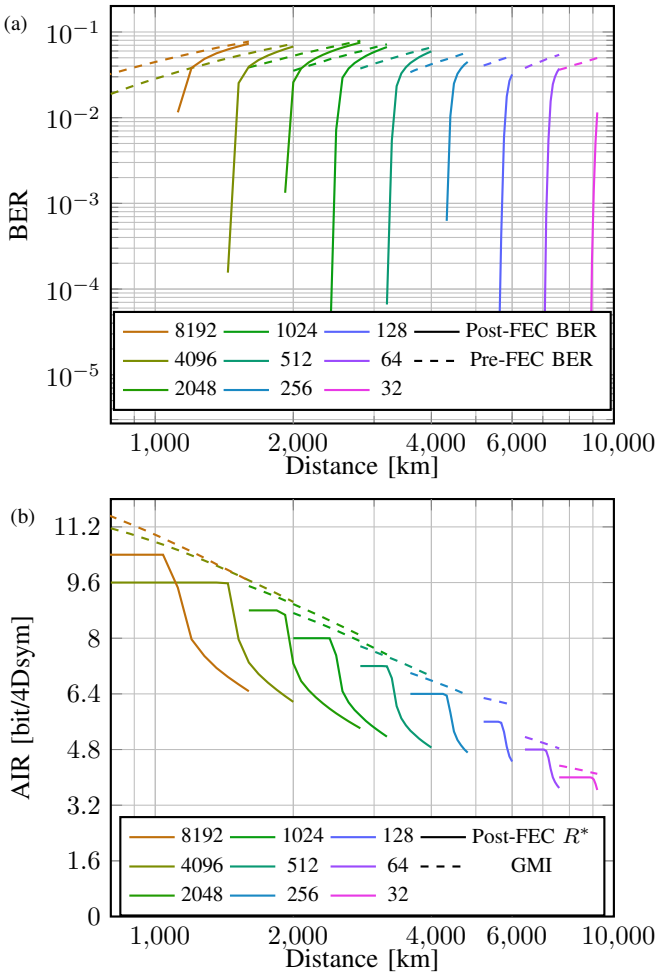

Fig. 6. Comparisons of the GS-4D constellations shaped for the AWGN channel. (a) shows the pre- and post-FEC BER for the $R = 4/5$ DVB-S2 LDPC and (b) shows the GMI and the post-FEC rate vs the transmitted distance. Numbers in the legend indicate the constellation order M.

the same SSFM simulation setup as described in Sec. V-B. The constellations were designed to maximise the trade-off between shaping gain and nonlinear distortion. This was achieved by numerical optimisation, again using the trust-region algorithm, using Eq. (34) as the objective function. The eta ratio c was estimated to be around 0.4, established by fitting the performance difference between quadrature phase shift keyed (QPSK) transmission and transmission where the sequence was drawn from a normal distribution as the reference distribution. These results present a range of constellations for a fixed eta ratio since the performance increase is not guaranteed if this changes. For a given system, where the length, number of amplifiers and spectral neighbours are fixed, these constellations show an improvement in performance. The lower cardinality constellations perform better for longer distances and saturate for shorter distances. The GMI saturates to m, the R^* saturates to mR. At the target reach, the R^* gets close to the GMI, this is the SNR for which the constellations were optimised.

The comparison of the different strategies investigated in

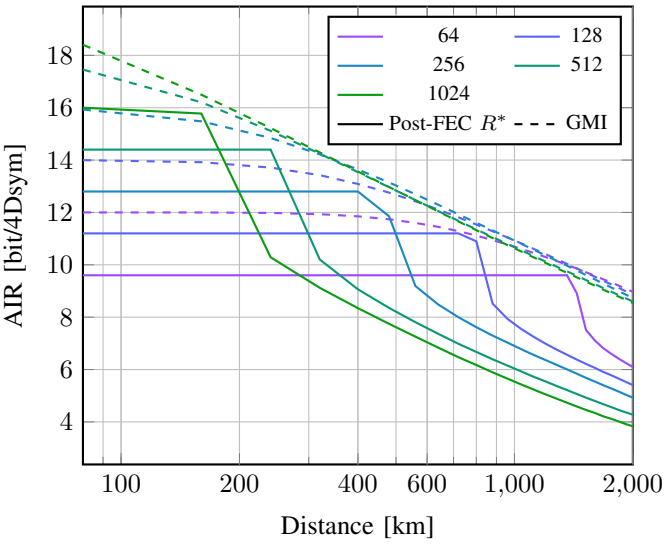

Fig. 7. Comparison of the GS-NL-2D constellations, which are shaped to trade off linear and nonlinear shaping gain, designed for $R = 4/5$ code. The GMI (dashed lines) and the post-FEC rate R^* are plotted against the transmitted distance. Numbers in the legend indicate the constellation order.

© 2022 IEEE. Personal use is permitted, but republication/redistribution requires IEEE permission. See https://www.ieee.org/publications/rights/index.html for more information.
Authorized licensed use limited to: University College London. Downloaded on August 17,2022 at 14:04:44 UTC from IEEE Xplore. Restrictions apply.

This article has been accepted for publication in IEEE/OSA Journal of Lightwave Technology. This is the author's version which has not been fully edited and content may change prior to final publication. Citation information: DOI 10.1109/JLT.2022.3197366

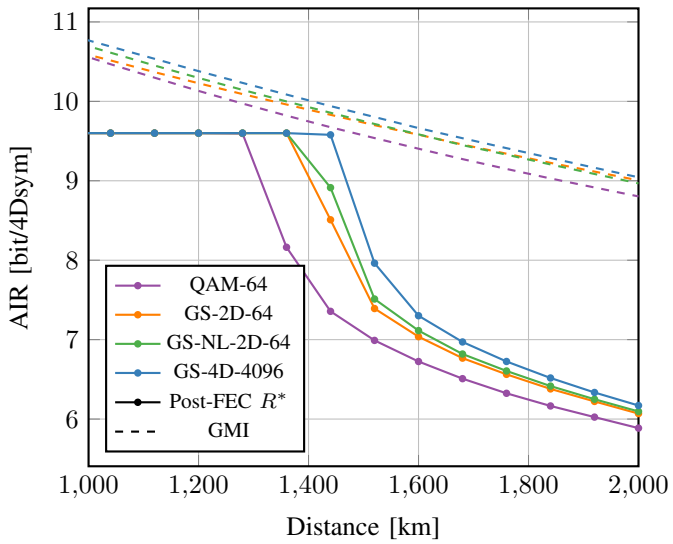

Fig. 8. Comparison of constellation formats with 64 points per 2D. The GMI and the post-FEC rate R^* are plotted versus the transmitted distance.

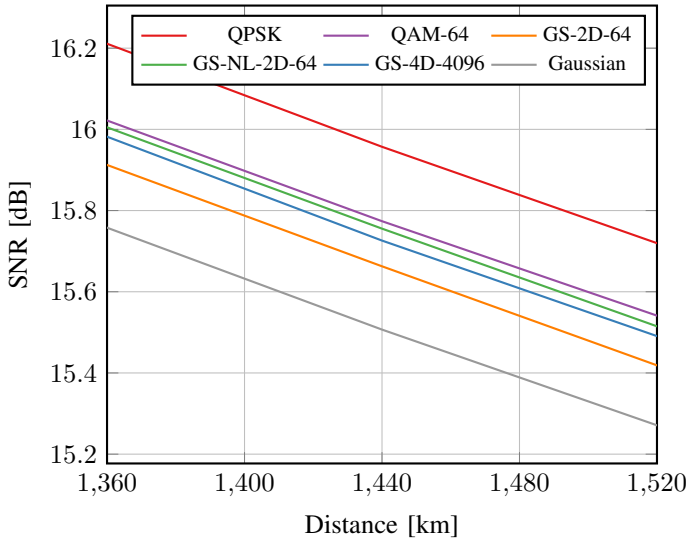

Fig. 9. Comparison of transmission performance for constellations with 64 points per 2D. The achievable SNR for QPSK and Gaussian modulation is shown for reference.

this paper is shown in Fig. 8 evaluated using the SSFM as described previously. This figure shows the performance of 4 different formats, namely the regular square QAM, 2D and 4D constellations optimised for the AWGN channel and a 2D constellation optimised with the same number of bits per 4 dimensions, in terms of the trade-off between the linear and nonlinear shaping gain. All curves saturate for shorter transmitted distances, the GMI at $m = 12$ bit/4D and the R^* at $mR = 9.6$ bit/4D. The first result shown is regular QAM. Following this, the 2D constellation shaped for AWGN is presented, which exhibits better performance. The 2D constellation shaped for the linear/nonlinear trade-off has a slightly better performance. The 4D constellation for AWGN has the best performance in terms of AIR. it should be noted that although it does not show the best performance in terms of SNR, it results in a higher AIR or throughput, in terms of GMI, through the resultant shaping gain. The nonlinear performance metrics presented in this paper are only valid for 2D constellations and, therefore, applying these metrics to the 4D constellation yielded no further performance improvements and the reason why is the subject of current research [42]. It can be seen, however, that all the shaped constellations outperform the regular QAM, after a 1520-km transmission; the 4D constellation by 0.27 bit/4D, the constellation shaped for the nonlinear channel with 0.18 bit/4D and the 2D constellation shaped for AWGN by 0.16 bit/4D in GMI. The R^* shows that the GS-4D-4096 has a reach increase of 2 spans, whereas the GS-2D and the GS-NL-2D show a reach increase of more than 1 span, where after 1440 km transmission, the GS-NL-2D outperforms the GS-2D by 0.4 bit/4D.

The performance in terms of SNR for each constellation, is shown in Fig. 9. With the SNR results, we can explain some of the performance differences in Fig. 8. The results also show the SNR for QPSK and Gaussian modulation for comparison, as these represent the reasonable best and worst nonlinear channel responses, respectively. For the reference case of Gaussian modulation, the transmitted sequence was generated with samples taken from a normal distribution, treated as symbols.

The effect of each constellation format on the nonlinear performance can be observed. As expected, the square QAM performed the best and the GS-2D constellation shaped for the AWGN channel performs the worst with 0.1 dB between them. However, the GS-2D constellation still outperformed the square QAM by at least one span or 0.1 bit higher GMI.

It can be seen that the GS-4D constellation has the best performance overall. The constellation exhibits very good nonlinear performance despite not being optimised for nonlinearity, increasing the SNR at optimum launch power. Together with excellent shaping gain from the additional degrees of freedom, this 4D AWGN-optimised constellation was the best performer in our selection.

For the case of the GS-NL-2D constellation, shaped using Eq. (34) as optimisation function, the nonlinear SNR penalty was reduced to a value close to that of the square 64-QAM whilst retaining shaping gain. The loss in shaping gain is more than offset by the improvement of the nonlinear channel response.

The drawback of the 4D constellation is that it requires a 4D demapper, meaning that instead of 2×64 2D distances, 4096 4D distances must be evaluated; a factor of 64 increase in the number of points and a factor of two again for the doubling in the number of the dimensions per constellation point. The choice of constellation thus becomes a trade-off between performance and complexity.

In Fig. 10, the geometrically shaped constellations are compared at the transmission distance of 1440 km. Here the launched power is swept and it can be seen that the optimum launch power is close to 0.5 dBm per channel used

© 2022 IEEE. Personal use is permitted, but republication/redistribution requires IEEE permission. See https://www.ieee.org/publications/rights/index.html for more information.
Authorized licensed use limited to: University College London. Downloaded on August 17,2022 at 14:04:44 UTC from IEEE Xplore. Restrictions apply.

This article has been accepted for publication in IEEE/OSA Journal of Lightwave Technology. This is the author's version which has not been fully edited and content may change prior to final publication. Citation information: DOI 10.1109/JLT.2022.3197366

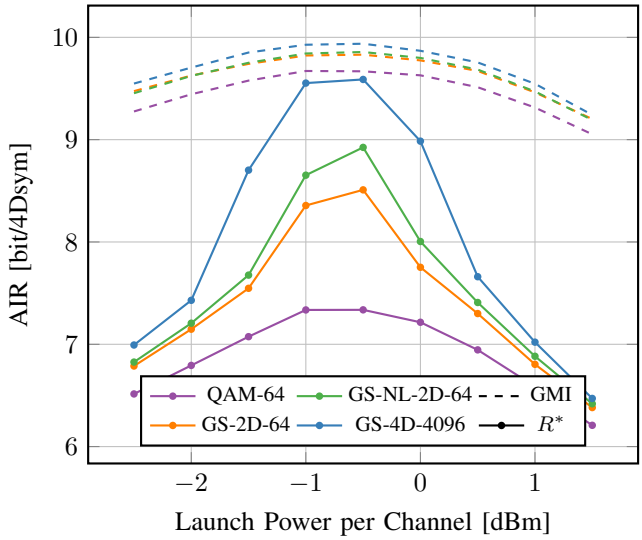

Fig. 10. Comparison of achievable rates for constellations with 64 points per 2D versus launch power at a transmission distance of 1440 km.

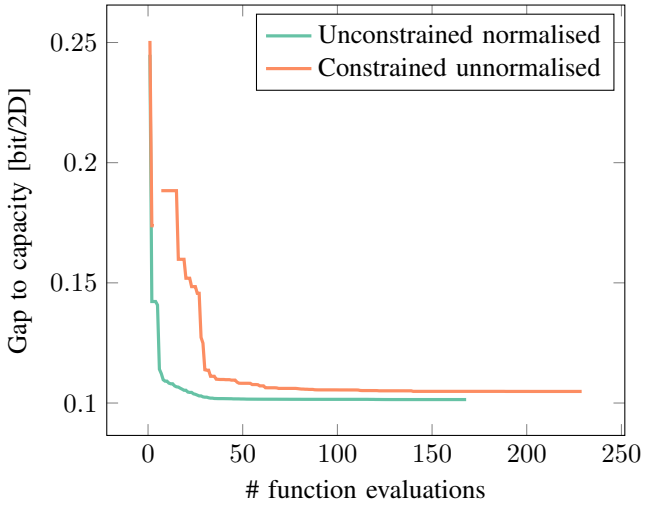

Fig. 11. Comparison of convergence speed between an unconstrained optimisation where the gradient includes normalisation and constrained optimisation where the gradient does not include the normalisation. Both optimising 1024 QAM for AWGN starting from APSK.

previously. The GS-NL-2D constellation outperforms the GS-2D even when the GMI is lower, suggesting that resulting LLRs result in better LDPC performance, although more research is necessary to reach a conclusion on that.

The choice between the GS-2D and GS-NL-2D would then depend on the system's operational consideration. When a system is expected to be fully loaded, the lesser impact on neighbouring channels of the GS-NL-2D may be attractive. When the system is expected to operate more sparsely, with lower nonlinear interaction between channels, the improved performance through maximising shaping gain with GS-2D can prove to be more beneficial. Ideally, this change should be applied in an adaptive manner, in response to the change in system conditions such as demand, transmission distances and the number of occupied wavelength channels.

VII. Computational Complexity

Whilst we optimise the geometry of the constellation, all constellation points influence each other and the performance of the constellation as a whole is measured by a single scalar metric, i.e., the MI or GMI. That means the objective function can be seen as a function that takes in an $M \times 2N$ matrix and outputs a scalar value. For some optimisation techniques, it is convenient to re-shape the input as a vector, this way the gradient and Hessian are defined.

The slowest operation in the calculation is the evaluation of Eq. (17) and the summation for GHQ. Fortunately, calculating the gradient in addition to the function does not require additional evaluations of Eq. (17), just an additional summation for the GHQ. This makes the evaluation of the function and gradient approximately two times slower than just evaluating the function. To investigate the scaling of the computational complexity, we can simply count how many times Eq. (17) is evaluated. For the MI, it is calculated for every i and every j multiplied by the number of points used for the GHQ. Therefore, if we have M constellation points and L GHQ points per dimension, the computational complexity scales with $\mathcal{O}(M^2 \times L^{2N})$. For GMI, the complexity scales with $\mathcal{O}\big(M^2 \times L^{2N} + \log_2(M) \times M \times \frac{M}{2} \times L^{2N}\big)$. When increasing the number of dimensions, the number of constellation points must grow exponentially with the number of dimensions if the number of bits per dimension is to remain constant. If we define $\hat{m} = \frac{\log_2(M)}{N}$ as the number of bits per 2 dimensions, then the GMI scales with $\mathcal{O}\big((2^{\hat{m}2N} + \hat{m}N \times 2^{\hat{m}4N}) \times L^{2N}\big)$.

Typically, the gradient of the function can be calculated using the finite difference method, which allows to obtain numerically the gradient for optimisation. For a single input and a single output, [48, Ch. 25] provides an expression for the calculation of finite differences. The derivative of a function g at a point x is approximated via the finite-difference method $(g(x+h) - g(x))/h$ for some small value of h. When the function takes multiple inputs, the procedure is repeated for every input variable. It is important to note that this method requires an extra function evaluation for every component of the input space. This will quickly become unfeasible; for example, optimising a 4D 4096-QAM constellation requires $4{\times}4096 = 16384$ evaluations of the objective function.

Our method, combining the normalisation with the objective function of the optimisation, allows us to use unconstrained optimisation methods. This is superior to using the MI or GMI with respect to an input constellation directly as an objective function and prevents the constellation amplitude from growing using a power constraint in the optimisation. This allows us to use unconstrained quasi-Newton optimisation algorithms, as shown in Fig. 11. In this example, 1024 QAM was optimised for the AWGN channel starting from an APSK constellation described in [43]. Another benefit of combining the gradient and channel constraint function this way is that it allows the channel function to include other channel effects, for example residual phase noise or device nonlinearities, beyond optical transmission systems.

© 2022 IEEE. Personal use is permitted, but republication/redistribution requires IEEE permission. See https://www.ieee.org/publications/rights/index.html for more information.
Authorized licensed use limited to: University College London. Downloaded on August 17,2022 at 14:04:44 UTC from IEEE Xplore. Restrictions apply.

This article has been accepted for publication in IEEE/OSA Journal of Lightwave Technology. This is the author's version which has not been fully edited and content may change prior to final publication. Citation information: DOI 10.1109/JLT.2022.3197366

VIII. Conclusions

This paper presents a novel and fast computation method for optimising geometrically shaped signal constellations with very high cardinality.

We proposed the use of an analytically derived gradient, instead of the conventionally-used finite-difference method, significantly reducing the complexity of numerical optimisation. Additionally, we combined the gradient of the mutual information with the Jacobian of the channel constraints, translating the problem into an unconstrained optimisation problem. We have successfully applied this technique to both linear and nonlinear optical communication systems.

We applied the proposed algorithms to show shaping gain for high cardinality 2- and 4- dimensional constellations, to generate geometrically shaped constellations, with up to 8192 constellation points. An 8192-ary constellation achieving a GMI with a gap of just 0.06 bit/2D to the AWGN channel capacity was designed, with the gains in mutual information verified using a simulation of a nonlinear optical fibre communication system, exhibiting shaping gains in both the linear and nonlinear regimes.

Although the focus herein is on optical communication systems, the same approach can be applied more generally to other types of communication systems. While undoubtedly useful for optical communications, these results can be applied to the design and optimisation of a wide range of transmission systems operating in linear- and nonlinear regimes.

Appendix A
Derivation of the Gradient of the MI

The gradient of the MI is a vector partial derivative

$$\nabla I = [\frac{\partial}{\partial \underline{x}_1} I, \frac{\partial}{\partial \underline{x}_2} I, \ldots, \frac{\partial}{\partial \underline{x}_M} I] \,. \tag{44}$$

To derive the gradient more easily we consider the different parts of the equation. First, we can define a function $g_i(\underline{z}, \boldsymbol{x}_{\mathcal{J}})$ for the MI and set $\widetilde{\mathcal{J}_i} = \{j \in \mathcal{J}; j \neq i\}$, which depends on $h(\underline{z}, \underline{x}_i, \underline{x}_j)$

$$\begin{aligned} g_i(\underline{z}, \boldsymbol{x}_{\mathcal{J}}) &\triangleq \log_2 \left(\sum_{j \in \mathcal{J}} h(\underline{z}, \underline{x}_i, \underline{x}_j) \right) \\ &= \log_2 \left(1 + \sum_{j \in \widetilde{\mathcal{J}_i}} h(\underline{z}, \underline{x}_i, \underline{x}_j) \right) \end{aligned} \tag{45}$$

$$h(\underline{z}, \underline{x}_i, \underline{x}_j) \triangleq \exp\left(\frac{||\underline{x}_i - \underline{x}_j||^2 + 2\langle \underline{z}, (\underline{x}_i - \underline{x}_j) \rangle}{-\sigma_z^2} \right) . \tag{46}$$

For these building blocks, the partial derivative can be easily obtained.

The partial derivatives in the gradient can be derived using the Leibniz and the chain rule:

$$\begin{aligned} \frac{\partial}{\partial \underline{x}_n} I = &-\frac{1}{M} \int_{\mathbb{R}^{2N}} f(\underline{z}) \frac{\partial}{\partial \underline{x}_n} g_n(\underline{z}, \boldsymbol{x}_{\mathcal{J}}) \mathrm{d}\underline{z} \\ &-\frac{1}{M} \sum_{i \in \widetilde{\mathcal{J}_n}} \int_{\mathbb{R}^{2N}} f(\underline{z}) \frac{\partial}{\partial \underline{x}_n} g_i(\underline{z}, \boldsymbol{x}_{\mathcal{J}}) \mathrm{d}\underline{z} \end{aligned} . \tag{47}$$

The sum over i is already split into the cases $i = n$ and $i \neq n$, which simplifies the next steps.

To evaluate this gradient, we start with the partial derivative of Eq. (45)

$$\frac{\partial}{\partial \underline{x}_n} g_i(\underline{z}, \boldsymbol{x}_{\mathcal{J}}) = \begin{cases} \frac{\sum_{j \in \widetilde{\mathcal{J}_n}} \frac{\partial}{\partial \underline{x}_n} h(\underline{z}, \underline{x}_n, \underline{x}_j)}{\log(2) \sum_{j \in \mathcal{J}} h(\underline{z}, \underline{x}_n, \underline{x}_j)} & \text{for } i = n \\ \frac{\frac{\partial}{\partial \underline{x}_n} h(\underline{z}, \underline{x}_i, \underline{x}_n)}{\log(2) \sum_{j \in \mathcal{J}}^{M} h(\underline{z}, \underline{x}_i, \underline{x}_j)} & \text{for } i \neq n \end{cases} , \tag{48}$$

with which we can then arrive to partial derivative of Eq. (46) as

$$\frac{\partial}{\partial \underline{x}_n} h(\underline{z}, \underline{x}_i, \underline{x}_j) = \begin{cases} 0 & \text{for } n = i \wedge n = j \\ \left(\frac{2\underline{d}_{nj} + 2\underline{z}}{-\sigma_z^2} \right) h(\underline{z}, \underline{x}_n, \underline{x}_j) & \text{for } n = i \wedge n \neq j \\ -\left(\frac{2\underline{d}_{in} + 2\underline{z}}{-\sigma_z^2} \right) h(\underline{z}, \underline{x}_i, \underline{x}_n) & \text{for } n \neq i \wedge n = j \\ 0 & \text{for } n \neq i \wedge n \neq j \end{cases} . \tag{49}$$

Considering we have a summation over i and a summation over j for every partial derivation toward x_j, we can identify 4 cases, two of which are trivial, where x_n does not appear or $x_i - x_j = x_n - x_n = 0$, the other two are very similar and can reuse partial results from the function evaluation, reducing the computational complexity.

Appendix B
Optimisation Algorithm

Algorithm 1 Bit labelling

$x \leftarrow \Re^{M \times 2N}$ ▷ *Constellation*
$m \leftarrow [m_1, \ldots, m_{2N}]$ ▷ *Number of bits per dimension*
procedure AssignLabels(x, m) ▷ *Map m bits to x*
  $i \leftarrow$ Argsort($x[:, 1]$)
  $D \leftarrow$ Ndim(x)
  if $D = 1$ **then**
    $l(i) \leftarrow$ Graymap(m)
      ▷ *Assign Gray map to 1D constellation.*
  else
    $l_{\mathrm{dim}} \leftarrow$ Graymap($m[1]$)
      ▷ *Labels for first dimension.*
    for $j \leftarrow 1, \ldots 2^{m[1]}$ **do**
      ▷ *Recursively label the other dimensions for each label seperately.*
      $M_j \leftarrow \prod_{d=2}^{D} 2^{m_d}$
        ▷ *Number labels in next dimensions.*
      $s \leftarrow i[M_j(j-1) + (1, \ldots, M_j)]$
        ▷ *Selection for this label.*
      $l_s \leftarrow$ AssignLabels($x[s, 2, \ldots, D], m[2, \ldots, D]$)
        ▷ *Labels for the selection.*
      $l[s] \leftarrow M_j l_{\mathrm{dim}}[j] + l_s$
        ▷ *Assign combination of labels.*
    end for
  end if
return l
end procedure

© 2022 IEEE. Personal use is permitted, but republication/redistribution requires IEEE permission. See https://www.ieee.org/publications/rights/index.html for more information.
Authorized licensed use limited to: University College London. Downloaded on August 17,2022 at 14:04:44 UTC from IEEE Xplore. Restrictions apply.

This article has been accepted for publication in IEEE/OSA Journal of Lightwave Technology. This is the author's version which has not been fully edited and content may change prior to final publication. Citation information: DOI 10.1109/JLT.2022.3197366

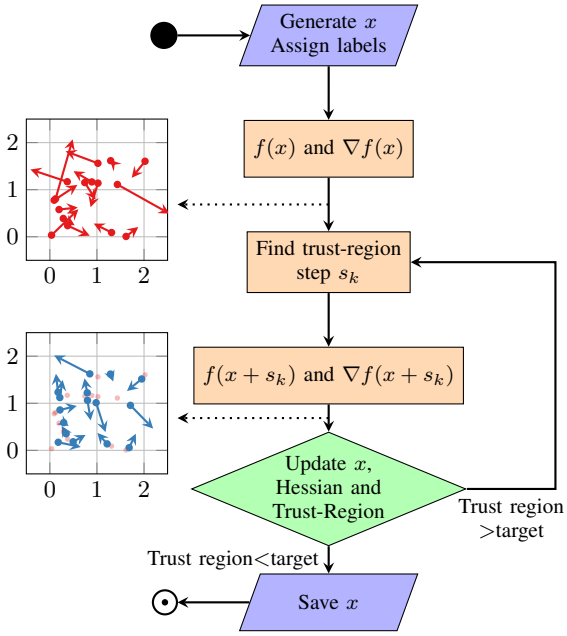

Fig. 12. Process workflow of the optimisation algorithm for constellation x. In this process we used Eq. (21) in Eq. (31) for $f(x)$ and Eq. (32) for $\nabla f(x)$. The insets show a single quadrant of the constellation and its gradient for x and $x + s_k$ of the first step.

The optimisation algorithm consists of two parts, first the initial constellation and second the trust-region optimisation. We found that generating a few constellations as a starting point, optimising them with the trust-region algorithm until the selected stopping condition is reached, and keeping only the best performing constellation gave good results.

For the initial constellation, there are a few options. First, there is the use of the known 'good' constellations and binary labellings. Herein we have used square QAM and constellations proposed in [43]. Alternatively, a lattice or a randomly generated constellation using a Gaussian prior as starting points were also used in this work. When using randomly assigned bit labels the optimisation algorithm converged to local minima, we only found good performance when bit labels were added. To obtain the bit labels, we have used the algorithm 1, for which we need the following definitions: If L is a list, then $\textsc{Argsort}(L)$ is the lexicographically least permutation of the indices $[0, ..., \textsc{Len}(L) - 1]$ such that $L[\textsc{Argsort}(L)]$ is sorted. The procedure $\textsc{Graymap}(m)$ returns the indices for a 1D Gray-coded constellation, e.g., $\textsc{Graymap}(2) = [0, 1, 3, 2]$ and $\textsc{Graymap}(3) = [0, 1, 3, 2, 6, 7, 5, 4]$.

When the bit labelling is obtained for the Cartesian coordinates of the constellation, the bit labels resemble the Gray-coded QAM. If fact, labelling a regular square constellation results in Gray-coded regular square QAM. Similarly, when the bit labelling is obtained for the N-dimensional spherical coordinates, the constellations resemble AS-PSK or the constellations proposed in [43]. We found that for lower SNR relative to the cardinality of the constellation, the latter performs better and for higher SNR the Cartesian basis for generating the bit labels works best.

The process of the trust-region optimisation is shown in Fig. 12. After generating a constellation and assigning bit labels to it, a trust-region algorithm is applied [40]. The algorithms start with calculating the function value and its gradient. The inverse Hessian B is assumed to be an identity matrix and the trust region to be of size 1. Steihaug's conjugate gradient method [41] is used to find trust-region step s_k and the function and gradient at $x+s_k$ are evaluated. The ratio between the actual reduction and the predicted reduction [40, Eq. (4.4)] is used to update the constellation and the trust region size. If it is greater than 0, the new x will be $x + s_k$, otherwise s_k is discarded. Note that the actual reduction can be negative and move the constellation away from its current local minimum. The size of the trust region is reduced or increased based on whether the ratio is below 0.2 or above 0.8 respectively. When the trust-region size has shrunk smaller than a set target (we used 3×10^{-4}) the optimisation is considered complete.

ACKNOWLEDGMENT

The authors are grateful to Dr Bin Chen for discussions on the topic of geometric constellation shaping and for sharing the coordinates of the OS-128 constellation.

REFERENCES

[1] A. Ghazisaeidi, I. F. d. Jauregui Ruiz, R. Rios-Muller, L. Schmalen, P. Tran, P. Brindel, A. C. Meseguer, Q. Hu, F. Buchali, G. Charlet, and J. Renaudier, "65Tb/s transoceanic transmission using probabilistically-shaped PDM-64QAM," in *European Conference on Optical Communication (ECOC) - Post Deadline Paper*, 2016.

[2] S. L. Olsson, J. Cho, S. Chandrasekhar, X. Chen, P. J. Winzer, and S. Makovejs, "Probabilistically shaped pdm 4096-qam transmission over up to 200 km of fiber using standard intradyne detection," *Opt. Express*, vol. 26, no. 4, pp. 4522–4530, Feb 2018.

[3] M. Ionescu, D. Lavery, A. Edwards, E. Sillekens, L. Galdino, D. Semrau, R. I. Killey, W. Pelouch, S. Barnes, and P. Bayvel, "74.38 Tb/s0 transmission over 6300 km single mode fiber with hybrid EDFA/Raman amplifiers," in *2019 Optical Fiber Communications Conference and Exhibition (OFC)*, 2019.

[4] L. Galdino, A. Edwards, W. Yi, E. Sillekens, Y. Wakayama, T. Gerard, W. S. Pelouch, S. Barnes, T. Tsuritani, R. I. Killey, D. Lavery, and P. Bayvel, "Optical fibre capacity optimisation via continuous bandwidth amplification and geometric shaping," *IEEE Photonics Technology Letters*, vol. 32, no. 17, pp. 1021–1024, 2020.

[5] Y. Wakayama, E. Sillekens, L. Galdino, D. Lavery, R. I. Killey, and P. Bayvel, "Increasing achievable information rates with pilot-based DSP in standard intradyne detection," in *European Conference on Optical Communication (ECOC)*, 2019.

[6] J. Cai, H. G. Batshon, M. V. Mazurczyk, O. V. Sinkin, D. Wang, M. Paskov, W. W. Patterson, C. R. Davidson, P. C. Corbett, G. M. Wolter, T. E. Hammon, M. A. Bolshtyansky, D. G. Foursa, and A. N. Pilipetskii, "70.46 Tb/s over 7,600 km and 71.65 Tb/s over 6,970 km transmission in C+L band using coded modulation with hybrid constellation shaping and nonlinearity compensation," *Journal of Lightwave Technology*, vol. 36, no. 1, pp. 114–121, 2018.

[7] R. T. Jones, T. A. Eriksson, M. P. Yankov, and D. Zibar, "Deep learning of geometric constellation shaping including fiber nonlinearities," in *European Conference on Optical Communication (ECOC)*, 2018.

[8] R.-J. Essiambre, R. Ryf, M. Kodialam, B. Chen, M. Mazur, J. Bonetti, R. Veronese, H. Huang, A. Gupta, F. A. Aoudia, E. Burrows, D. Grosz, L. Palmieri, X. Chen, N. K. Fontaine, H. Chen, and M. Sellathurai, "Increased reach of long-haul transmission using a constant-power 4d format designed using neural networks," in *European Conference on Optical Communication (ECOC)*, 2020, pp. Mo1E–5.

[9] V. T. abd Toshiaki Koike-Akino, Y. Wang, D. Millar, K. Kojima, and K. Parsons, "End-to-end deep learning for phase noise-robust multi-dimensional geometric shaping," in *European Conference on Optical Communication (ECOC)*, 2020, pp. Th1D–4.

© 2022 IEEE. Personal use is permitted, but republication/redistribution requires IEEE permission. See https://www.ieee.org/publications/rights/index.html for more information.
Authorized licensed use limited to: University College London. Downloaded on August 17,2022 at 14:04:44 UTC from IEEE Xplore. Restrictions apply.

This article has been accepted for publication in IEEE/OSA Journal of Lightwave Technology. This is the author's version which has not been fully edited and content may change prior to final publication. Citation information: DOI 10.1109/JLT.2022.3197366

[10] T. Fehenberger, A. Alvarado, G. Böcherer, and N. Hanik, "On probabilistic shaping of quadrature amplitude modulation for the nonlinear fiber channel," *Journal of Lightwave Technology*, vol. 34, no. 21, pp. 5063–5073, 2016.

[11] O. Geller, R. Dar, M. Feder, and M. Shtaif, "A shaping algorithm for mitigating inter-channel nonlinear phase-noise in nonlinear fiber systems," *Journal of Lightwave Technology*, vol. 34, no. 16, pp. 3884–3889, 2016.

[12] J. Renner, T. Fehenberger, M. P. Yankov, F. Da Ros, S. Forchhammer, G. Böcherer, and N. Hanik, "Experimental comparison of probabilistic shaping methods for unrepeated fiber transmission," *Journal of Lightwave Technology*, vol. 35, no. 22, pp. 4871–4879, 2017.

[13] E. Sillekens, D. Semrau, G. Liga, N. A. Shevchenko, Z. Li, A. Alvarado, P. Bayvel, R. I. Killey, and D. Lavery, "A simple nonlinearity-tailored probabilistic shaping distribution for square QAM," in *Optical Fiber Communication Conference*. Optical Society of America, 2018, p. M3C.4.

[14] S. Zhang, F. Yaman, E. Mateo, T. Inoue, K. Nakamura, and Y. Inada, "Design and performance evaluation of a gmi-optimized 32qam," in *European Conference on Optical Communication (ECOC)*, 2017.

[15] E. Sillekens, D. Semrau, D. Lavery, P. Bayvel, and R. I. Killey, "Experimental demonstration of geometrically-shaped constellations tailored to the nonlinear fibre channel," in *European Conference on Optical Communication (ECOC)*, 2018.

[16] B. Chen, A. Alvarado, S. van der Heide, M. van den Hout, H. Hafermann, and C. Okonkwo, "Analysis and experimental demonstration of orthant-symmetric four-dimensional 7 bit/4D-Sym modulation for optical fiber communication," pp. 2737–2753, 2021.

[17] H. Dzieciol, G. Liga, E. Sillekens, P. Bayvel, and D. Lavery, "Geometric shaping of 2-dimensional constellations in the presence of laser phase noise," *Journal of Lightwave Technology*, p. Preprint, 2020.

[18] L. M. Beda, L. N. Korolev, N. V. Sukkikh, and T. S. Frolova, "Programs for automatic differentiation for the machine BESM," Institute for Precise Mechanics and Computation Techniques, Academy of Science, Moscow, USSR, Technical Report, 1959, (In Russian).

[19] L. B. Rall, Ed., *Automatic Differentiation: Techniques and Applications*. Springer Berlin Heidelberg, 1981.

[20] G. Foschini, R. Gitlin, and S. Weinstein, "Optimization of two-dimensional signal constellations in the presence of gaussian noise," *IEEE Transactions on Communications*, vol. 22, no. 1, pp. 28–38, 1974.

[21] G. H. Golub and C. F. Van Loan, *Matrix Computations*, 3rd ed. Johns Hopkins, 1996.

[22] A. Splett, C. Kurtzke, and K. Petermann, "Ultimate transmission capacity of amplified optical fiber communication systems taking into account fiber nonlinearities," in *1993 The European Conference on Optical Communication (ECOC)*, 1993.

[23] P. Poggiolini, "The gn model of non-linear propagation in uncompensated coherent optical systems," *Journal of Lightwave Technology*, vol. 30, no. 24, pp. 3857–3879, 2012.

[24] R. Dar, M. Feder, A. Mecozzi, and M. Shtaif, "Properties of nonlinear noise in long, dispersion-uncompensated fiber links," *Opt. Express*, vol. 21, no. 22, pp. 25 685–25 699, Nov 2013.

[25] R. Dar *et al.*, "On shaping gain in the nonlinear fiber-optic channel," *IEEE International Symposium on Information Theory*, pp. 2794–2798, June 2014.

[26] D. Semrau, R. I. Killey, and P. Bayvel, "A closed-form approximation of the gaussian noise model in the presence of inter-channel stimulated raman scattering," *J. Lightwave Technol.*, vol. 37, no. 9, pp. 1924–1936, May 2019.

[27] D. Semrau, E. Sillekens, R. I. Killey, and P. Bayvel, "A modulation format correction formula for the gaussian noise model in the presence of inter-channel stimulated Raman scattering," *J. Lightwave Technol.*, vol. 37, no. 19, pp. 5122–5131, Oct 2019.

[28] C. E. Shannon, "A mathematical theory of communication," *Bell System Technical Journal*, vol. 27, no. 3, pp. 379–423, 1948.

[29] T. M. Cover and J. A. Thomas, *Elements of Information Theory*, 2nd ed. Wiley, Apr. 2005. [Online]. Available: https://doi.org/10.1002/047174882x

[30] G. Caire, G. Taricco, and E. Biglieri, "Bit-interleaved coded modulation," *IEEE Transactions on Information Theory*, vol. 44, no. 3, pp. 927–946, 1998.

[31] A. Alvarado, T. Fehenberger, B. Chen, and F. M. J. Willems, "Achievable information rates for fiber optics: Applications and computations," *J. Lightwave Technol.*, vol. 36, no. 2, pp. 424–439, Jan 2018.

[32] C. G. Broyden, "The convergence of a class of double-rank minimization algorithms 1. general considerations," *IMA Journal of Applied Mathematics*, vol. 6, no. 1, pp. 76–90, 1970.

[33] R. Fletcher, "A new approach to variable metric algorithms," *The Computer Journal*, vol. 13, no. 3, pp. 317–322, Mar. 1970.

[34] D. Goldfarb, "A family of variable-metric methods derived by variational means," *Mathematics of Computation*, vol. 24, no. 109, pp. 23–23, Jan. 1970.

[35] D. F. Shanno, "Conditioning of quasi-Newton methods for function minimization," *Mathematics of Computation*, vol. 24, no. 111, pp. 647–647, Sep. 1970.

[36] T. F. Coleman and Y. Li, "An interior trust region approach for nonlinear minimization subject to bounds," *SIAM Journal on Optimization*, vol. 6, no. 2, pp. 418–445, may 1996.

[37] R. H. Byrd, R. B. Schnabel, and G. A. Shultz, "A trust region algorithm for nonlinearly constrained optimization," *SIAM Journal on Numerical Analysis*, vol. 24, no. 5, pp. 1152–1170, 1987.

[38] R. H. Byrd, H. F. Khalfan, and R. B. Schnabel, "Analysis of a symmetric rank-one trust region method," *SIAM Journal on Optimization*, vol. 6, no. 4, pp. 1025–1039, nov 1996.

[39] A. R. Conn, N. I. M. Gould, and P. L. Toint, "Convergence of quasi-newton matrices generated by the symmetric rank one update," *Mathematical Programming*, vol. 50, no. 1, pp. 177–195, Mar 1991.

[40] J. Nocedal and S. Wright, *Numerical Optimization*, 2nd ed. Springer New York, 2006.

[41] T. Steihaug, "The conjugate gradient method and trust regions in large scale optimization," *SIAM Journal on Numerical Analysis*, vol. 20, no. 3, pp. 626–637, 1983.

[42] G. Liga, A. Barreiro, H. Rabbani, and A. Alvarado, "Extending fibre nonlinear interference power modelling to account for general dual-polarisation 4d modulation formats," *Entropy*, vol. 22, no. 11, 2020.

[43] H. Méric, "Approaching the gaussian channel capacity with APSK constellations," *IEEE Communications Letters*, vol. 19, no. 7, pp. 1125–1128, July 2015.

[44] Feng-Wen Sun and H. C. A. van Tilborg, "Approaching capacity by equiprobable signaling on the gaussian channel," *IEEE Transactions on Information Theory*, vol. 39, no. 5, pp. 1714–1716, Sep. 1993.

[45] G. Forney, R. Gallager, G. Lang, F. Longstaff, and S. Qureshi, "Efficient modulation for band-limited channels," *IEEE Journal on Selected Areas in Communications*, vol. 2, no. 5, pp. 632–647, 1984.

[46] C. Menyuk, "Nonlinear pulse propagation in birefringent optical fibers," *IEEE Journal of Quantum Electronics*, vol. 23, no. 2, pp. 174–176, 1987.

[47] *Digital Video Broadcasting (DVB); Second generation framing structure, channel coding and modulation systems for Broadcasting, Interactive Services, News Gathering and other broadband satellite applications; Part 2: DBV-S2 Extensions (DVB-S2X)*, European Standard ETSI EN 302 307-2, 2014.

[48] M. Abramowitz and I. A. Stegun, *Handbook of mathematical functions with formulas, graphs and mathematical tables*, 9th ed. New York: Dover, 1965.

© 2022 IEEE. Personal use is permitted, but republication/redistribution requires IEEE permission. See https://www.ieee.org/publications/rights/index.html for more information.
Authorized licensed use limited to: University College London. Downloaded on August 17,2022 at 14:04:44 UTC from IEEE Xplore. Restrictions apply.